



Article

Impacts of Urban Green Space on Land Surface Temperature from Urban Block Perspectives

Hongmin An ¹, Hongyan Cai ², Xinliang Xu ² , Zhi Qiao ³ and Dongrui Han ^{4,*} ¹ School of Management, Shandong University, Jinan 250100, China² State Key Laboratory of Resources and Environmental Information System, Institute of Geographic Sciences and Natural Resources Research, Chinese Academy of Sciences, Beijing 100101, China³ School of Environmental Science and Engineering, Tianjin University, Tianjin 300350, China⁴ Institute of Agricultural Information and Economics, Shandong Academy of Agricultural Sciences, Jinan 250100, China

* Correspondence: handr@reis.ac.cn

Abstract: Urban green space (UGS) can be regarded as an effective approach to mitigate urban heat island (UHI) effects. Many studies have investigated the impacts of composition and configuration of UGS on land surface temperature (LST), while little attention has been paid to the impacts among different urban blocks. Thus, taking 1835 urban blocks in Beijing as samples, including low-rise point (LRP), low-rise street (LRS), low-rise block (LRB), mid-rise point (MRP), mid-rise street (MRS), mid-rise block (MRB), high-rise point (HRP), high-rise street (HRS) and high-rise block (HRB), this study investigated the impacts of UGS on LST among different urban blocks. The results showed that UGS serves as cold islands among different urban blocks. Percentage of landscape (PLAND) of UGS in all types of urban blocks, edge density (ED) of UGS in MRS, area-weighted fractal dimension index (FRAC_AM) of UGS in HRS and HRB show significantly negative impacts on LST, while aggregation index (AI) of UGS in LRP shows significantly positive impacts. The findings suggest that both composition and configuration of UGS can affect LST among different urban blocks and rational allocation of UGS would be effective for mitigating UHI effects.

Keywords: urban green space; land surface temperature; urban blocks; composition and configuration



Citation: An, H.; Cai, H.; Xu, X.; Qiao, Z.; Han, D. Impacts of Urban Green Space on Land Surface Temperature from Urban Block Perspectives.

Remote Sens. **2022**, *14*, 4580.

<https://doi.org/10.3390/rs14184580>

Academic Editors: Weiqi Zhou, Xiaolian Liu and Zhonghao Zhang

Received: 10 August 2022

Accepted: 10 September 2022

Published: 13 September 2022

Publisher's Note: MDPI stays neutral with regard to jurisdictional claims in published maps and institutional affiliations.



Copyright: © 2022 by the authors. Licensee MDPI, Basel, Switzerland. This article is an open access article distributed under the terms and conditions of the Creative Commons Attribution (CC BY) license (<https://creativecommons.org/licenses/by/4.0/>).

1. Introduction

Urban heat island (UHI) is the phenomenon that the temperature in urban areas is significantly higher than that in the suburbs [1,2]. It is widely accepted that urbanization is the primary factor contributing to UHI effects, while UHI leads to negative impacts on the urban climate and dwellers, such as increased energy consumption, increased pollutant concentration, increased health issues and reduced thermal comfort of urban dwellers [3–9]. Noteworthy, with the development of urbanization, the negative impacts will be further exacerbated [10,11]. Therefore, mitigating the UHI effects is of great significance in improving urban climate and thermal comfort.

With the development of remote sensing technology, a series of images, such as Moderate Resolution Imaging Spectroradiometer (MODIS), Visible Infrared Imaging Radiometer Suite (VIIRS), Landsat and ECOSystem Spaceborne Thermal Radiometer Experiment on Space Station (ECOSTRESS), have the advantages of wide cover range, real time and rapidity, which can provide credible and fundamental data for land surface temperature (LST) research [12–15]. Furthermore, due to different temporal and spatial resolutions, these data have been widely used for LST research at city, nation and global scales [12,16–19]. These studies have provided a better understanding of monitoring LST changes and influence mechanisms of UHI effects.

Urban landscapes, such as impervious surface, water bodies and vegetation, have been recognized as the main factor affecting the UHI [20,21]. Numerous studies have

investigated the impacts of urban landscapes on LST [20,22,23]. Generally, impervious surface can enhance surface sensible heat flux, which leads to increase LST [10,24,25]. On the contrary, water bodies and vegetation can decrease LST, and the main reasons are high heat capacity and evaporative cooling of the former and increasing latent heat flux of the latter, respectively [3,23,26]. Therefore, the reasonable allocation of landscapes has become one of the effective measures to mitigate the UHI effects [27,28].

Urban green space (UGS), which is mainly composed of all types of vegetation, such as grasslands, forests and green belts, is considered as an effective approach to mitigate the UHI effects [28–34]. Many scholars have investigated the impacts of UGS on LST, noting that UGS can significantly reduce LST [4,35–37]. This is mainly because UGS can affect humidity and albedo of land surface, which leads to reduce LST [38–40]. It is emphasized that both composition and configuration of UGS can affect LST [29,32,41]. Generally, it is widely accepted that the higher amount of UGS the better the cooling effect [32,41,42]. For example, Mahyar and Puar (2019) [32] investigated the impacts of spatial pattern of UGS on LST and emphasized that increasing the amount of UGS can reduce LST. Zhou and Cao (2020) [42] also found that UGS has a significantly negative correction with LST in summer. Furthermore, configuration (e.g., shape, aggregation and connectivity) of UGS is emphasized as another key factor, which can also influence LST. Generally, the more complex the shape of UGS, the better the cooling effect [41,43,44]. Additionally, studies pointed out that different aggregation of UGS has different impacts on LST. For example, Estoque et al. (2017) [23] investigated the relationship between the spatial pattern of UGS and LST, noting that the aggregation of UGS has a positive relationship with LST. Kong et al. (2016) [45] found that as the aggregation of UGS increases, LST increases initially and then decreases. Similar to aggregation, the connectivity of UGS also has different impacts on LST. For example, Asgarian et al. (2015) [46] and Chen et al. (2014) [47] emphasized that UGS with higher connectivity can increase the cooling effect, whereas Li et al. (2013) [43] and Zhou et al. (2011) [48] observed the opposite effect.

Existing studies have investigated the impacts of UGS on LST, and the analysis scales mainly focus on grid, city and region [25,32,49,50]. However, little attention has been given to urban block scale. Generally, cities are composed many urban blocks, including many landscapes, especially buildings with different heights and layouts, which can significantly affect thermal environment [51]. It also brings great challenges for UGS planning in mitigating UHI effects among different urban blocks. Therefore, it is necessary to investigate the impacts of UGS on LST among different urban blocks.

Landscape indices, which can reflect landscape pattern characteristics, are widely used to quantify the spatial composition and configuration of landscapes. Composition indices, such as percentage of landscape (PLAND) and total landscape area (TA), can quantify the abundance and variety of landscape [52]. Configuration indices, such as landscape shape index (LSI), interspersion juxtaposition index (IJI) and aggregation index (AI), can quantify spatial distribution and arrangement of landscape [36,42,52]. These two types of indices can not only describe different aspects of the landscape, but also complement each other [35,52]. Therefore, both composition and configuration indices were applied to characterize the UGS structure in this study.

The aim of this study is to explore the differences of UGS characteristics influencing LST from urban block perspectives. The main objects of this study were (1) to analyze the spatial pattern of LST and UGS; (2) to investigate the composition of UGS among different urban blocks; (3) to analyze the LST difference between urban blocks and UGS; and (4) to explore the impacts of UGS on LST among different urban blocks. This study provides scientific guidance to urban planners on how to mitigate the UHI effects among different urban blocks through the rational allocation of UGS.

2. Materials and Methods

2.1. Study Area

Beijing is the capital of China ($39^{\circ}26'–41^{\circ}03'N$, $115^{\circ}25'–117^{\circ}30'E$), and it covers an area of 16,410 km² (Figure 1). Since the 1978 economic reform and opening-up policy, Beijing has experienced rapid urbanization, which has accelerated the transformation from natural surface into impervious surface. By the end of 2019, Beijing's population reached 21.54 million, with an urbanization ratio of 87.53%. High urbanization level makes Beijing become one of the most severe UHI effects cities in China.

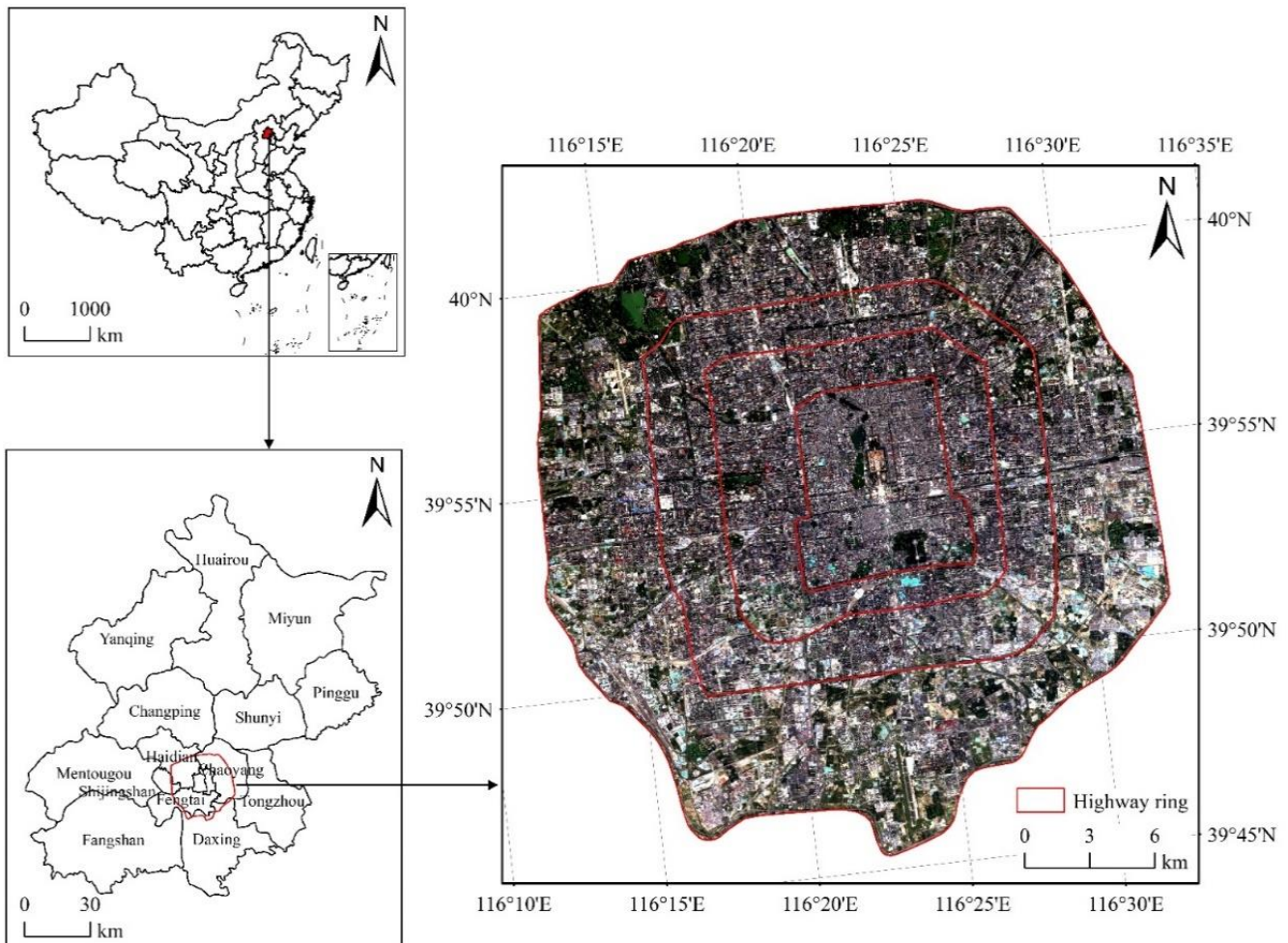


Figure 1. Location of the study area.

The study area is located within the 5th ring road, which covers an area of approximately 668 km² (Figure 1). Although this region comprises only 4.07% of the total area of Beijing, it has the highest urbanization level. In particular, due to rapid urbanization, urban surface landscapes, especially three-dimensional buildings (low-rise, mid-rise and high-rise buildings), have changed drastically, which significantly affects urban ventilation conditions and thermal environment [5,7,53–56]. Therefore, the diversity of buildings made this region a good choice for investigating the impacts of UGS on LST among different urban blocks.

2.2. Data Sources

Urban blocks dataset, Gaofen1 (GF1) image, Landsat 8 OLI image and meteorological data were used in this study.

Urban blocks dataset was derived from Beijing City Laboratory (BCL). Eleven attributes, such as ID of the block, number of buildings and types of street block form, are

included in this dataset. Taking building floors and density as classification criteria, urban blocks were classified into nine categories, including low-rise point (LRP), low-rise street (LRS), low-rise block (LRB), mid-rise point (MRP), mid-rise street (MRS), mid-rise block (MRB), high-rise point (HRP), high-rise street (HRS) and high-rise block (HRB), and the details can be seen in Table 1. In this study, nine types of urban blocks in Beijing were extracted to investigate the impacts of UGS on LST among different urban blocks.

Table 1. Classification criteria of urban blocks.

Types	Building Floors	Building Density
LRP	1–3	0–0.15
LRS	1–3	0.15–0.25
LRB	1–3	>0.25
MRP	4–7	0–0.15
MRS	4–7	0.15–0.25
MRB	4–7	>0.25
HRP	≥8	0–0.15
HRS	≥8	0.15–0.25
HRB	≥8	>0.25

GF1 image was derived from Resources and Environmental Scientific Data Center (RESDC) and Chinese Academy of Sciences (CAS) and the acquisition dates was 19 September 2020. Four multi-spectral bands (blue, green, red and near infrared) were included in this image, with a spatial resolution of 16 m, and the image was cloud-free in the study area. The image was used to extract precise UGS because it has better spatial resolution than Landsat image.

Landsat 8 OLI image was acquired from the United States Geological Survey (USGS) on 7 August 2020. The thermal infrared band (band10), which had a spatial resolution of 120 m, was used to retrieve the LST. In particular, the image was cloud-free, which can guarantee the accuracy of further processing.

Meteorological data were derived from China Meteorological Administration. Meteorological variables, such as air temperature, precipitation and wind speed, are included in this data. Given the acquisition time of the Landsat image was 10:52 (GMT + 8), therefore, hourly observed air temperature at 20 meteorological stations was extracted to validate the retrieved LST.

2.3. Methods

The flowchart of this study is as follows (Figure 2). First, UGS was extracted by a GF1 image based on object-oriented method, and LST was retrieved from a Landsat 8 OLI image based on image-based method (IBM). Second, urban blocks samples were selected based on UGS and urban block dataset. Third, spatial distribution of LST and UGS were analyzed. Fourth, composition of UGS among different urban blocks was analyzed. Fifth, LST difference between urban blocks and UGS were analyzed. Finally, the impacts of composition and configuration of UGS on LST among different urban blocks were investigated.

2.3.1. Extraction of UGS

Object-oriented method was used to extract UGS based on GF1 image [57,58]. Firstly, a multiresolution segmentation method was used to determine optimal segmentation scale. After repeated tests, the optimal segmentation scale, shape and compactness were determined as 10, 0.4 and 0.5, respectively. Secondly, UGS samples, which were acquired from Google Map and Baidu Map were selected and classification rules were established based on image information, including spectrum, texture and shape. Finally, neighbor algorithm was applied to extract UGS. To verify the accuracy of UGS, 500 samples were randomly selected. Taking Google Map as criteria, the accuracy of UGS was 92.80%. It can guarantee the accuracy of UGS for further analysis.

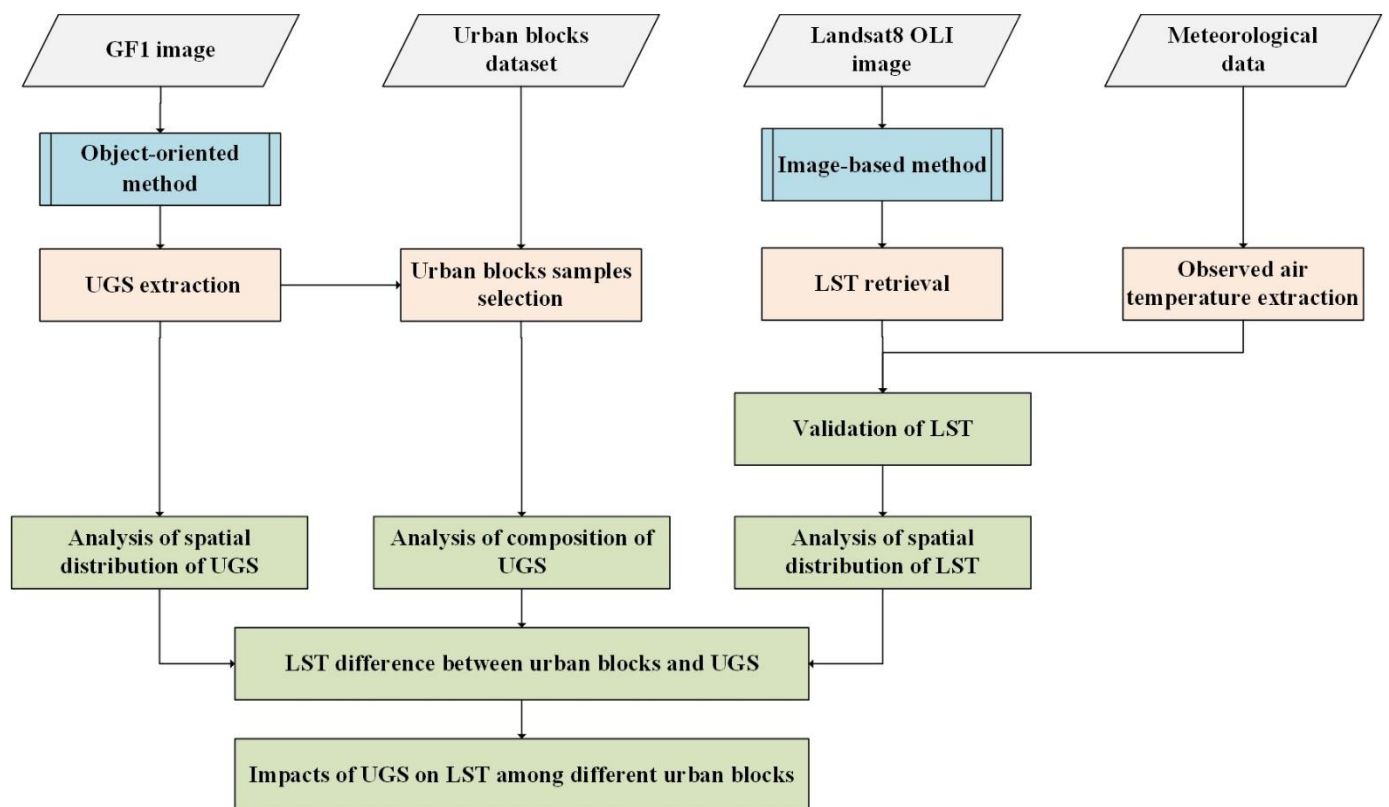


Figure 2. Flowchart of this study.

2.3.2. Selection of Urban Block Samples

To investigate the impacts of UGS on LST among different urban blocks, nine types of urban blocks were used in this study. Given the area of urban blocks and percentage of interior UGS, urban block samples were selected as follows. Firstly, percentage of interior UGS in each urban block were calculated. Secondly, blocks with an area greater than 15,000 m² and percentage of UGS greater than 1% were selected. Finally, 1835 urban blocks, including LRP (289), LRS (193), LRB (339), MRP (84), MRS (226), MRB (333), HRP (62), HRS (161) and HRB (148), were selected as samples to investigate the impacts of UGS on LST (Table 2), and the spatial distribution of urban block samples is shown in Figure 3.

Table 2. The number of different types of urban block samples.

Types	Number	Proportion
LRP	289	15.75%
LRS	193	10.52%
LRB	339	18.47%
MRP	84	4.58%
MRS	226	12.32%
MRB	333	18.15%
HRP	62	3.38%
HRS	161	8.77%
HRB	148	8.07%

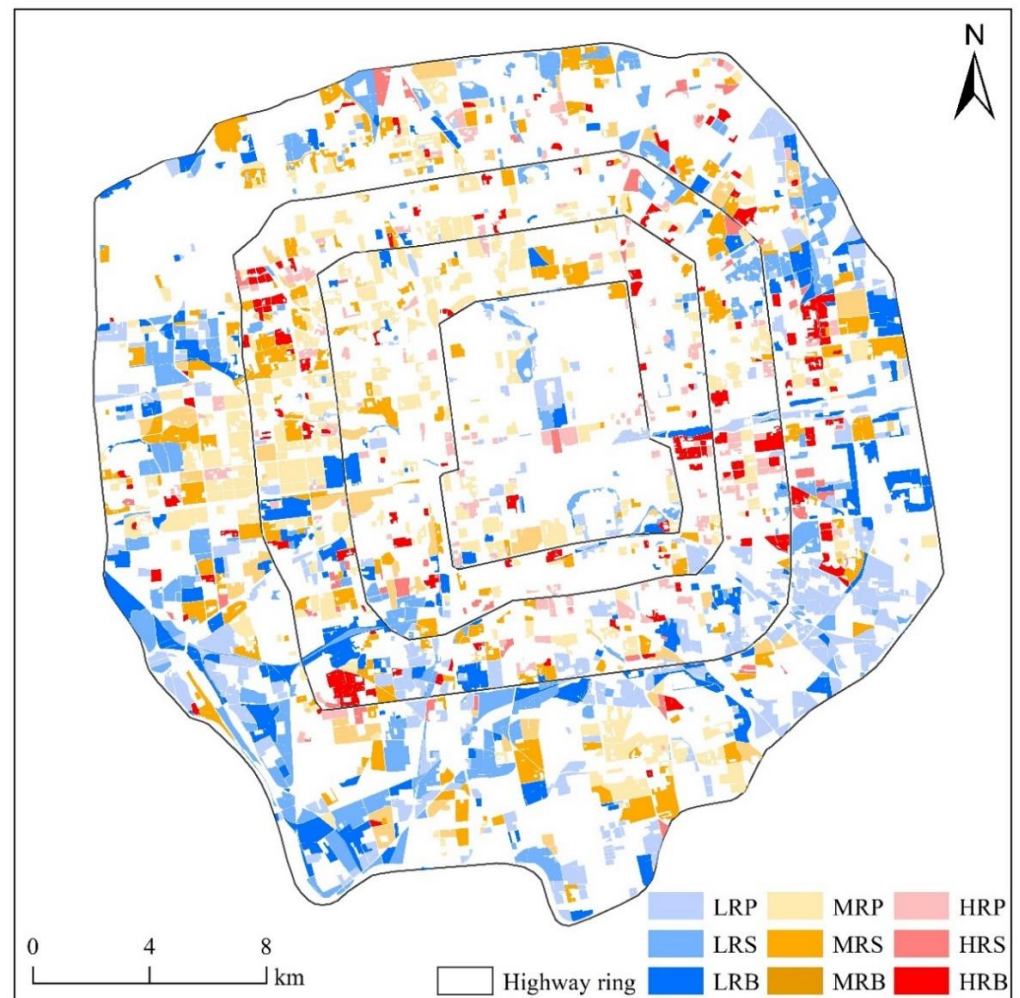


Figure 3. Spatial distribution of urban block samples.

2.3.3. Retrieval of LST

Image-based method (IBM) is used to retrieve the LST [39]. The formula is as follows:

$$T_s = \frac{T}{1 + \left(\frac{\lambda T}{\rho}\right) \ln \varepsilon} \quad (1)$$

where T_s is the LST, T represents the at-satellite brightness temperature, λ and ε are wavelength at the center of emitted radiance and spectral emissivity, respectively. ρ is a constant value derived from the headed files of Landsat 8 OLI image. In this case, ρ equals 1.438×10^{-2} mK.

To calculate T , radiation should be first determined. Radiation is converted by the digital number (DN) of thermal band (band 10), and the formula is as follows:

$$L\lambda = ML \times DN + AL \quad (2)$$

where $L\lambda$ is the spectral radiance ($\text{W}\cdot\text{m}^{-2}\cdot\text{sr}^{-1}\cdot\mu\text{m}^{-1}$), ML and AL are rescaled gain (value = 3.3420×10^{-4}) and rescaled bias (value = 0.1).

After calculating $L\lambda$, the T can be calculated as follows:

$$T = \frac{K_2}{\ln\left(\frac{K_1}{L\lambda} + 1\right)} \quad (3)$$

where $K_1 = 480.89 \text{ W}\cdot\text{m}^{-2}\cdot\text{sr}^{-1}\cdot\mu\text{m}^{-1}$ and $K_2 = 1201.14 \text{ K}$.

ε is a key parameter in LST retrieval, and it is crucial to retrieval of LST accurately. Usually, estimation of ε can also be divided into two steps. First, the land surface is classified into three groups, including water, urban, and natural surface. Then, the ε of water is set as 0.995, while for urban and natural surface, the ε can be calculated by fractional vegetation cover (*FVC*) (Equations (4) and (5)) [14,59]. The *FVC* is calculated by *NDVI* (Equation (6)).

$$\varepsilon_{urban} = 0.9589 + 0.086FVC - 0.0671FVC^2 \quad (4)$$

$$\varepsilon_{natural\ surface} = 0.9625 + 0.0614FVC - 0.0461FVC^2 \quad (5)$$

$$FVC = \frac{NDVI - NDVI_s}{NDVI_v - NDVI_s} \quad (6)$$

where ε_{urban} and $\varepsilon_{natural\ surface}$ are the emissivity values for urban and natural surface, respectively. *FVC* is the fractional vegetation cover. $NDVI_s$ and $NDVI_v$ are the *NDVI* for the vegetation and soil, respectively.

2.3.4. Analytical Methods

To explore the impacts of UGS on LST among different urban blocks, a stepwise regression model was used to choose the best fit explaining variance. Some metrics, including composition metric (PLAND) and configuration metrics (ED, area-weighted fractal dimension index (FRAC_AM), IJI, and AI), which are used to illustrate the structure of UGS, are selected as explanatory variables to explain LST among different urban blocks [23,29,32,36]. In particular, PLAND represents quantitative characteristics. ED and FRAC_AM represent shape complexity characteristics, and IJI and AI represent spatial aggregation characteristics. These metrics can be calculated by Fragstats 4.2, and the details are shown in Table 3.

Table 3. Description of landscape metrics.

Landscape Metrics	Description
PLAND	The proportion of a landscape occupied by patches of a given type, a measure of dominance.
ED	The total edge length of a given patch type per unit area (hectare), a measure of overall shape complexity.
FRAC_AM	The patch fractal dimension weighted by relative patch area, a measure of shape complexity of individual patches.
IJI	A measure of the degree to which the corresponding patch type is equally adjacent to all other patch types.
AI	The number of joins divided by the maximum possible number of joins involving a given patch type, multiplied by 100, a measure of the level of lumpiness of patches in a landscape.

3. Results

3.1. Validation of LST

To validate the precision of LST, observed air temperature at 20 meteorological stations was extracted and average retrieved LST were calculated from the 5×5 grid cells near the meteorological station. The relationship between observed air temperature and retrieved LST was compared, as shown in Figure 4. The result shows that LST and observed air temperature is highly correlated, with R^2 of 0.99. The RMSE of 2.75, and the mean difference is -2.54 °C, indicating that retrieved LST is higher than the observed air temperature. Although there are differences between observed air temperature and retrieved LST, it has high consistency. Therefore, the retrieved LST is reliable, which can reflect changes of LST accurately.

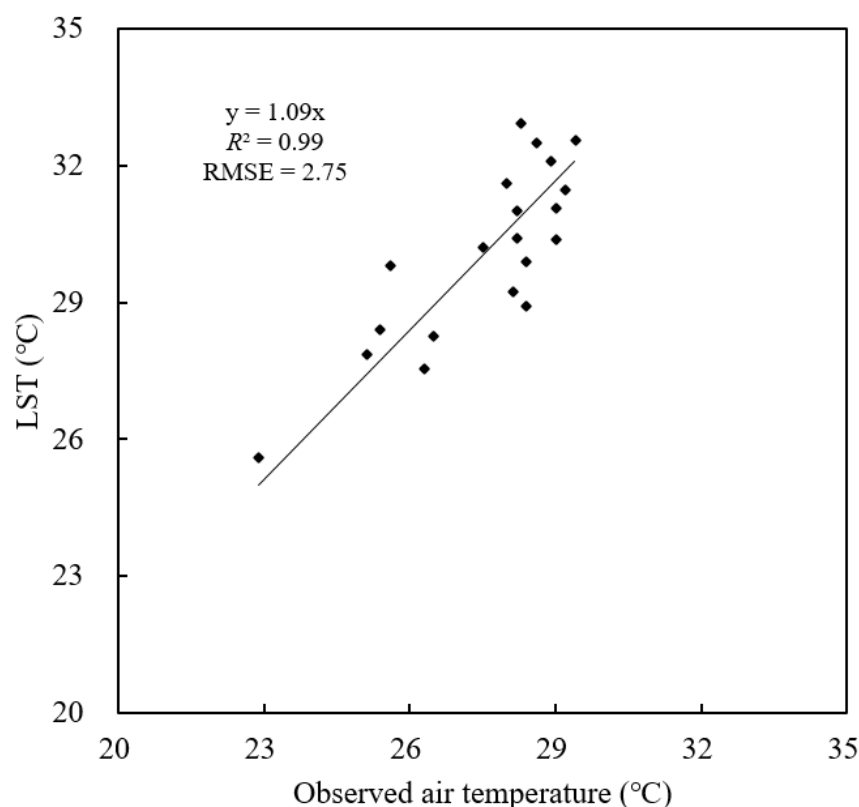


Figure 4. Relationship between observed air temperature and retrieved LST.

3.2. Spatial Distribution of UGS and LST

The spatial distribution of UGS and LST is shown in Figure 5. The result shows that both UGS and LST have significant spatial differences. Figure 5a shows the spatial distribution of UGS, and UGS is mainly distributed within the Fifth Ring Road, especially in parks, such as Summer Palace, Old Summer Palace and Olympics Park, where it is scattered within the Fourth Ring Road. The LST of the study area ranged from 24.87 °C to 47.98 °C, with an average LST of 37.48 °C (Figure 5b). The LST shows a pattern of “high in the central and low in the surrounding areas”. The high LST is located in the central area, especially in the Second Ring Road, while low in the northwest and northeast of the study area. Obviously, there are many buildings and impervious surfaces in the central area of the study area, while many parks are located in the surrounding areas. Therefore, the LST of UGS is relatively lower than other landscape types, indicating that UGS serves as cold islands in the study area.

3.3. Composition of UGS among Different Urban Blocks

Table 4 shows the composition of UGS among different urban blocks. The result shows that the average proportion of UGS in low-density (building density lower than 0.15) blocks is the highest, followed by middle-density (building density ranged from 0.15 to 0.25) blocks, and high-density (building density higher than 0.25) blocks is the lowest. For low-rise blocks, the average proportion of UGS in LRP, LRS and LRB are 48.98%, 39.36% and 26.85%, respectively. Additionally, the average proportion of UGS in mid-rise blocks and high-rise blocks are similar to low-rise blocks. For mid-rise blocks, the average proportion of UGS in MRP, MRS and MRB are 42.07%, 27.21%, and 14.43%, respectively. For high-rise blocks, the average proportion of UGS in HRP, HRS and HRB are 36.26%, 22.47% and 14.79%, respectively. Therefore, the coverage of UGS decreases as the building density increases.

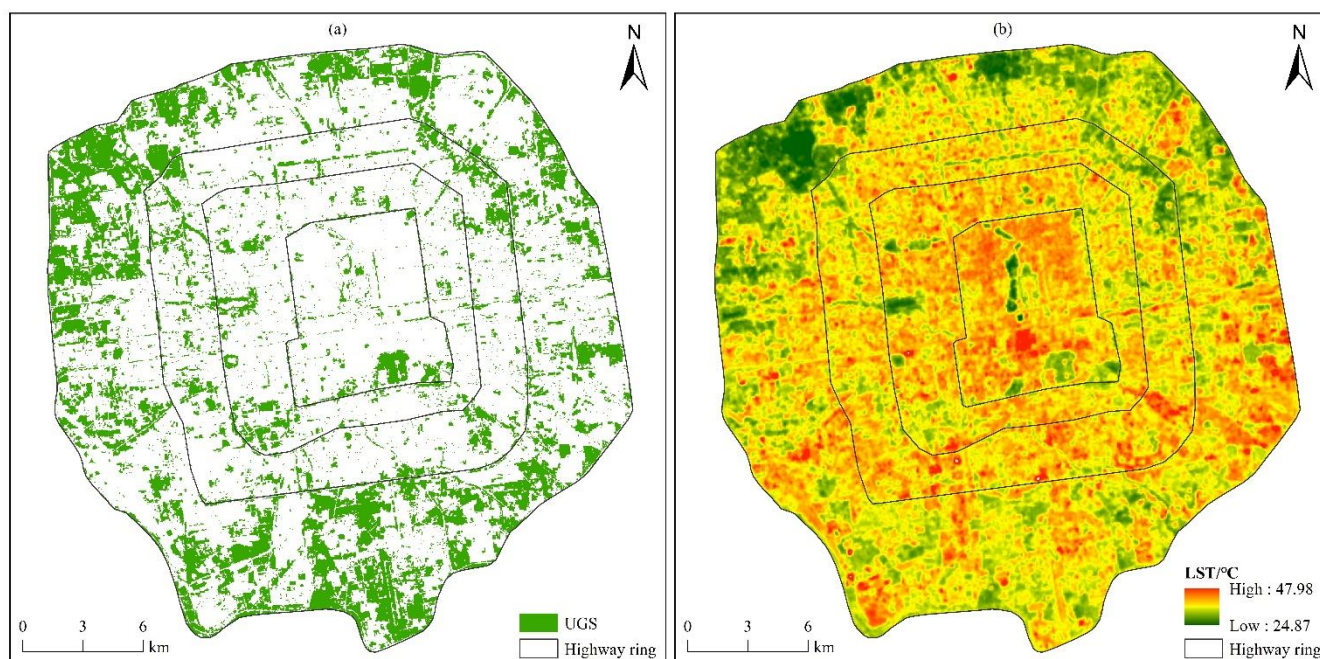


Figure 5. Spatial distribution of UGS and LST in the study area. (a) UGS; (b) LST.

Table 4. Composition of UGS among different urban blocks.

Types	Proportion of UGS		
	Minimum	Maximum	Average
LRP	3.41%	99.97%	48.98%
LRS	1.00%	79.40%	39.36%
LRB	0.66%	73.59%	26.85%
MRP	5.40%	96.87%	42.07%
MRS	1.56%	80.42%	27.21%
MRB	1.41%	72.77%	14.43%
HRP	1.55%	81.26%	36.26%
HRS	1.91%	81.94%	22.47%
HRB	1.41%	96.87%	14.79%

3.4. LST Difference between Urban Blocks and UGS

To investigate LST difference between urban blocks and UGS, average LST in each urban block and UGS were calculated and boxplot was shown in Figure 6. The result shows that there are significant differences in LST between urban blocks and UGS. Obviously, average LST in UGS is lower than that in urban blocks. In the study area, average LST ranged from 36.31 °C (HRP) to 38.48 °C (MRB) in urban blocks and ranged from 35.91 °C (HRP) to 37.66 °C (MRB) in UGS. It indicated that UGS plays the role of a cooling island in urban blocks. Additionally, average LST in urban blocks and UGS have a positive relationship with building density, indicating that the higher the building density, the higher the LST.

Moreover, LST difference varies with building density among different urban blocks. Comparing different density types, LST differences in low-density blocks is the lowest, followed by middle-density blocks and high-density blocks is the highest.

Furthermore, it is obvious that LST difference increases as building floors increase. LST difference in low-rise (building floor ranged from 1 to 3) blocks is the highest, followed by mid-rise (building floor ranged from 4 to 7) blocks and high-rise (building floor higher than 7) blocks is the least.

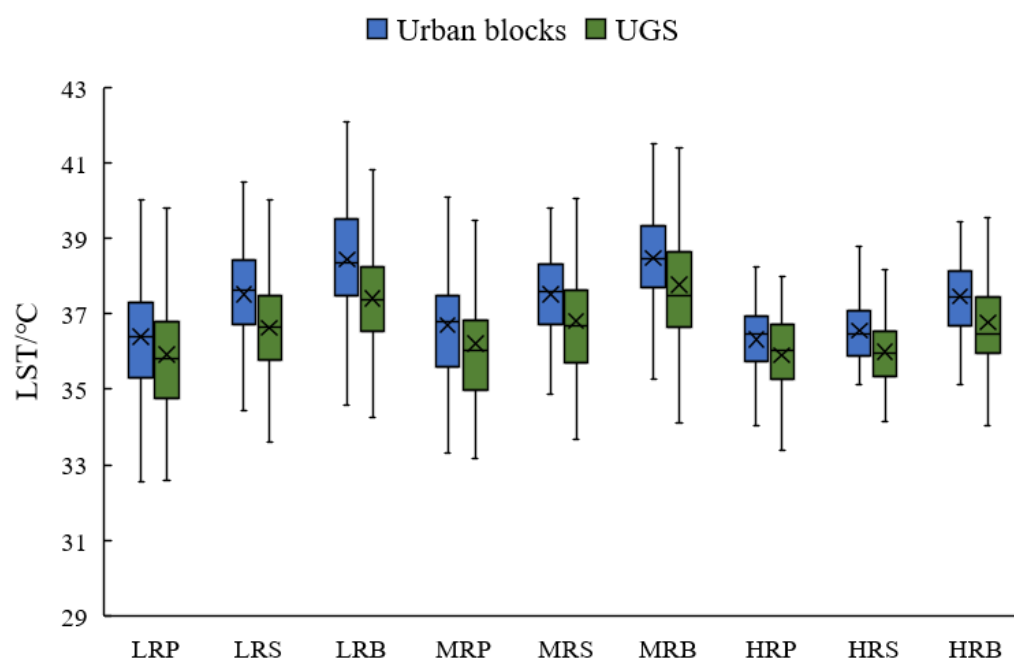


Figure 6. Comparison of LST between urban blocks and UGS.

3.5. Impacts of UGS on LST among Different Urban Blocks

Both composition (PLAND) and configuration (ED, FRAC_AM, IJI and AI) variables were used to investigate the impacts of UGS on LST among different urban blocks, and the key characteristics of UGS influencing LST among different urban blocks were identified (Table 5). The result shows that both the composition and configuration of UGS influences LST, and the contribution of UGS to LST varies among different urban blocks. Additionally, it should be noted that PLAND of UGS shows significantly negative impacts on LST in all types of urban blocks, while configuration variables of UGS show different impacts on LST among different urban blocks. In particular, IJI of UGS was not found to have a significant impact on LST in all types of urban blocks.

Table 5. Impacts of composition and configuration variables of UGS on LST among different urban blocks.

Types	Variables	Standardized Coefficient	R ²
LRP	PLAND	−0.55 **	0.22
	AI	0.23 **	
LRS	PLAND	−0.43 **	0.18
LRB	PLAND	−0.48 **	0.23
MRP	PLAND	−0.46 **	0.20
MRS	PLAND	−0.39 **	0.24
	ED	−0.20 **	
MRB	PLAND	−0.41 **	0.17
HRP	PLAND	−0.46 **	0.20
HRS	PLAND	−0.29 **	0.13
	FRAC_AM	−0.19 *	
HRB	PLAND	−0.41 **	0.15
	FRAC_AM	−0.16 *	

** Correlation is significant at the 0.01 level (two-tailed). * Correlation is significant at the 0.05 level (two-tailed).

For low-rise urban blocks, the PLAND and AI of UGS in LRP are significantly related to LST, while only one composition variable (PLAND) of UGS in LRS and LRB is significantly related to LST (Table 5). On average, 21% of low-rise urban blocks' LST is explained by the composition and configuration of UGS. Particularly, the PLAND of UGS has significantly negative impacts on LST, while the AI of UGS has positive impacts on LST. The LRP,

PLAND and AI of UGS can explain 22% of the variance in LST, and the PLAND and AI of UGS show significantly negative and positive impacts on LST, respectively, indicating that UGS with large density and low aggregation leads to decreased LST. For LRS and LRB, the PLAND of UGS can explain 18% and 23% of the variance in LST, and it has significant negative impacts on LST, suggesting that the larger the UGS density is, the lower the LST.

For mid-rise urban blocks, the PLAND and ED of UGS in MRS are significantly related to LST, while only one composition variable (PLAND) of UGS in MRP and MRB is significantly related to LST (Table 5). On average, 20% of mid-rise urban blocks' LST is explained by the composition and configuration of UGS. Particularly, the PLAND and ED of UGS have significantly negative impacts on LST. The MRS, PLAND and ED of UGS can explain 24% of the variance in LST, and the PLAND and ED of UGS show significantly negative impacts on LST, indicating that UGS with large density and high edge density lead to decrease LST. For MRP and MRB, the PLAND of UGS can explain 20% and 17% of the variance in LST, and it has significant negative impacts on LST, suggesting that the larger the UGS density is, the lower the LST.

For high-rise urban blocks, the PLAND and FRAC_AM of UGS in HRS and HRB are significantly related to LST, while only one composition variables (PLAND) of UGS in HRP is significantly related to LST (Table 5). On average, 16% of high-rise urban blocks' LST is explained by the composition and configuration of UGS. Particularly, the PLAND and FRAC_AM of UGS have significantly negative impacts on LST. For HRS and HRB, the PLAND and FRAC_AM of UGS can explain 13% and 15% of the variance in LST, and the PLAND and FRAC_AM of UGS have significantly negative impacts on LST, indicating that UGS with large density and high area weighted mean fractal dimension leads to decreased LST. For HRP, the PLAND of UGS can explain 20% of the variance in LST, and it has significant negative impacts on LST, suggesting that the larger the UGS density is, the lower the LST.

4. Discussion

4.1. Contribution of UGS to LST

Many studies have pointed out that UGS has cooling effects [28–34,60,61]. However, the contribution of UGS to LST is not clear. To further investigate the contribution, contribution index (CI), which refers to the degree of contribution (heating or cooling) of landscape to the thermal environment, was used in this study [62,63]. CI equals LST difference between UGS and urban blocks multiplies percentage of UGS in urban blocks. The positive and negative value of CI indicated that UGS is heating or cooling the LST. The spatial distribution of CI among different urban blocks is shown in Figure 7. The result shows that UGS has significant cooling effects in urban blocks, and the CI of UGS has significant spatial differences.

The CI of UGS ranged from -0.003 to -0.35 among different urban blocks, with an average CI of -0.10 , indicating that UGS can significantly decrease LST (Figure 7). High CI of UGS is mainly distributed in central areas, such as the 2nd and 3rd Ring Roads, while it is low within the 5th Ring Road. It indicated that UGS has better cooling effects in the surrounding areas than that in the central areas because LST in the central areas is high in the daytime. There are also differences in the CI of UGS among different urban blocks. The CI of UGS in LRB, MRS, MRB, MRP, HRP, HRS and HRB are mainly between -0.1 and 0 , while in other urban blocks it is mainly between -0.2 and -0.1 . The number of blocks with CI between -0.1 and 0 of UGS in LRB, MRS, MRB, HRP, HRS and HRB are 193, 128, 288, 25, 113 and 127, with the proportion of 56.93%, 56.64%, 86.49%, 40.32%, 70.19 and 85.81%, respectively, indicating that UGS has low cooling effects in most of these urban blocks. For LRP, LRS and MRP, the number of stations with CI between -0.2 and -0.1 of UGS are 118, 87 and 36, with the proportion of 40.83%, 45.08 and 42.86%, respectively, suggesting that UGS has better cooling effects in most of these urban blocks.

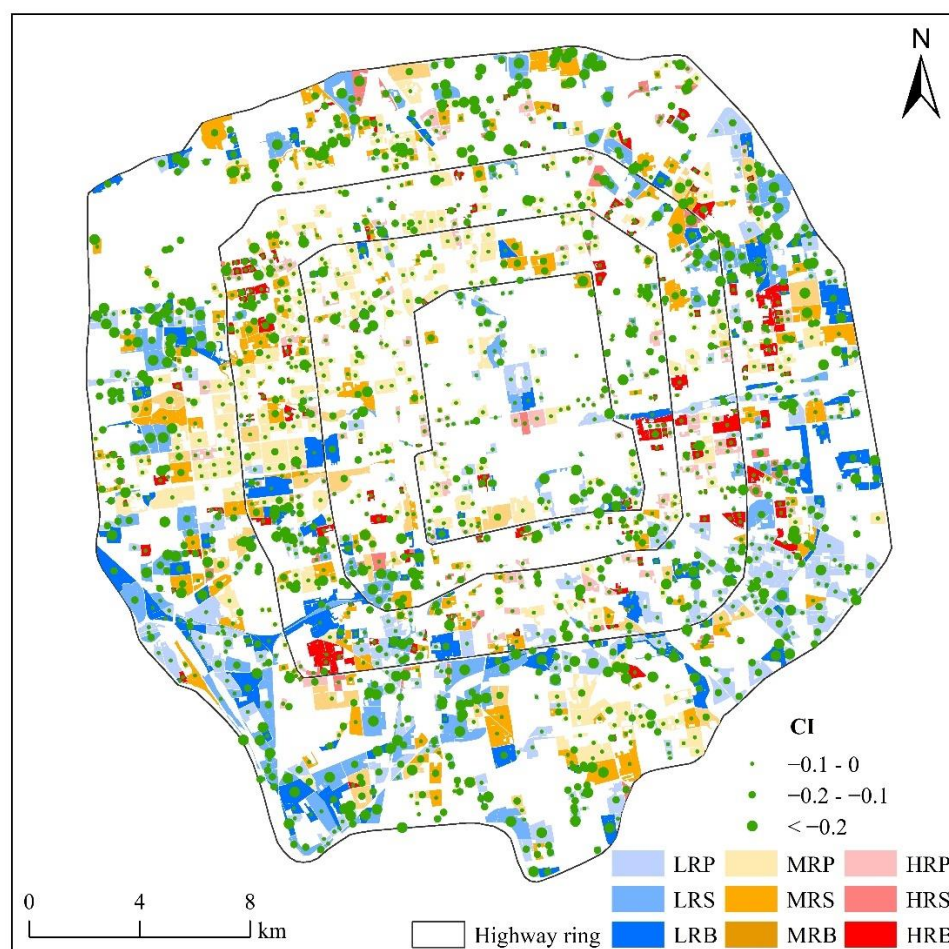


Figure 7. Spatial distribution of CI among different urban blocks.

4.2. Comparisons with Other Studies

Previous studies have investigated the impacts of UGS on LST, noting that UGS plays the key role in mitigating the UHI effects. Generally, the analysis scales of existing studies were mainly focus on grid, city and region [25,32,49,50]. For example, for grid scale, NDVI was widely used to chosen as the indicator to examine the relationship between UGS and LST, and a negative correlation were observed [64]. The impacts were explored in city (e.g., Beijing, Penang and Brisbane) and region scale (e.g., Singapore and Southeast Asia), and pointed out that UGS can effectively mitigate UHI effects [25,32,50,65]. However, little attention has been given to the impacts from urban blocks perspectives, and how UGS plays a role in LST among different urban blocks is also unclear. Urban block is the basic unit of urban fabric, and there are buildings with different heights and layouts in an urban block, which can significantly affect thermal environment [51]. Therefore, this study adopted urban block as an analysis scale for investigating the impacts, which is different from previous studies. We believe that our finding can provide a new perspective on mitigating the UHI effects on block scale.

It is emphasized that both composition and configuration of UGS can affect LST, and our findings observed it at the block scale, which is in line with previous studies [29,32,41]. However, our findings highlight that the role of UGS in mitigating the UHI effects varies with urban blocks types. For composition variable, the proportion of UGS has negative impacts on LST [32,41,42], and our findings emphasized that the PLAND of UGS has significantly negative impacts on LST in all types of urban blocks. It is consistent with previous studies [32,41,42]. For configuration variables, our findings emphasized that the composition of UGS affects LST in some types of urban blocks, which is different from previous studies. Our results showed that the increased shape complexity of UGS in MRS,

HRS and HRB can effectively reduce LST because the increased shape complexity of UGS can promote energy exchange between vegetation and building area, resulting in cooling the LST [41,66]. Our results showed that the increased aggregation of UGS in LRP can effectively increase LST. As Kong et al. (2014) [45] reported, discrete UGS has better cooling effect. Though there is no configuration variable of UGS in other urban types, it does not invalidate our results.

4.3. Implications for UGS Planning and UHI Mitigation

UGS is recognized as an effective approach to mitigate the UHI effects [28–32]. Our findings emphasized that both the composition and configuration of UGS can affect LST, and the impacts vary with different types of urban blocks [29,32,41]. Therefore, differential UGS planning for UHI mitigation should be implemented among different urban blocks.

In general, the higher the proportion of UGS, the better the cooling effect [32,41,42]. In this study, it is found that the PLAND of UGS has significantly negative impacts on LST in all types of urban blocks. It also provides a potential approach to mitigate UHI effects. Therefore, the increasing proportion of UGS should be taken into reasonable account in the future. Given the limited availability of lands for UGS in the Beijing metropolitan area, some strategies, such as roof and vertical greening, can be taken into account [67–69].

Moreover, our findings emphasized that the spatial configuration of UGS shows different impacts on LST among different urban blocks. This is mainly because that the configuration of UGS can affect the energy flow between different landscapes [70,71]. For low-rise blocks, UGS with low aggregation in LRS contributes to decrease LST. The more discrete the UGS, the better the cooling effect. For MRS, the ED of UGS is the key configuration variable. Our finding suggested that UGS with high edge density can significantly reduce LST. Increasing the length of UGS boundaries can effectively mitigate LST. Unlike low-rise and mid-rise blocks, high-rise blocks usually have better ventilation conditions due to more shade and large intervals of high-rise buildings [7,72–74]. On the one hand, high-rise buildings create more shade, which can change the impervious ability to absorb and emit energy, contributing to a cooling effect [36]. On the other hand, large intervals of high buildings facilitate the heat diffusion outward, leading to decreased LST [41]. Our finding also pointed out that the FRAC_AM of UGS is the key configuration variable in HRS and HRB, and it has significant negative impacts on LST. Increasing the complexity of UGS boundaries can be regarded as an effective approach to mitigate LST. However, there is no significant contribution of the configuration variable of UGS to LST in other urban blocks. Therefore, the reasonable planning of UGS among different urban blocks should be taken into account in the future.

4.4. Limitations

In this study, a Landsat 8 OLI image was used to retrieve LST during summer daytime, and UGS was generated based on a GF1 image. Considering the vigorous UGS growth, the strongest UHI effects and data availability, the impacts of UGS on LST were investigated in summer. However, this impact of UGS on LST during the day is still not investigated because nighttime LST data are lacking, and seasonal impacts should be further investigated. Additionally, this study was carried out in a typical urbanization city (Beijing). Although UHI effects is severe in the Beijing metropolitan area, the impacts of UGS on LST among different urban blocks may vary in different cities, such as inland cities and coastal cities. The impacts in other cities should be further investigated. Furthermore, both composition and configuration variables were used to quantitatively characterize the UGS structure, and its impacts on LST were investigated. However, LST is not affected by UGS, but also by many landscape factors, such as landscapes (e.g., water, impervious surface and road), urban morphology (e.g., building height, sky view factor and frontal area index) and meteorology (e.g., relative humidity, rainfall and wind) [25,55,75,76]. Due to data availability, these factors were not taken into account in this study, and it should be further investigated to comprehensively understand the impacts.

5. Conclusions

Taking Beijing as the study area, this study explored the impacts of UGS on LST among different urban blocks based on GF1 image, Landsat 8 OLI image, urban block dataset and meteorological data. The key characteristics of UGS influencing LST among different urban blocks were identified.

The results show that both UGS and LST have significant spatial differences. Average LST is significantly lower than urban blocks, indicating that UGS serves as cold islands in the study area. Both the composition and configuration of UGS can affect LST, and the contribution of UGS to LST varies among different urban blocks. The PLAND of UGS in all types of urban blocks, the ED of UGS in MRS, the FRAC_AM of UGS in HRS and the HRB show significantly negative impacts on LST, while the AI of UGS in LRP shows significantly positive impacts. It is emphasized that the reasonable planning of composition and configuration of UGS should be taken into account in designing different types of urban blocks in the future. The findings can extend the scientific understanding of the impacts of UGS characters on LST among different urban blocks. It provides guidance on optimizing UGS among different types of urban blocks for urban planners.

Author Contributions: Conceptualization, H.A. and D.H.; methodology, H.A. and D.H.; software, H.C., X.X. and Z.Q.; resources, H.C. and X.X.; writing—original draft preparation, H.A.; writing—review and editing, H.A. and D.H.; supervision, D.H. All authors have read and agreed to the published version of the manuscript.

Funding: This research was funded by the National Natural Science Foundation of China (Grant No. 41971389 and 41871138), Strategic Priority Research Program of the Chinese Academy of Sciences (Grant No. XDA20010302), Agricultural Science and Technology Innovation Project of Shandong Academy of Agricultural Sciences (Grant No. CXGC2022E07) and Key R & D Plan of Shandong Province (Major Scientific and Technological Innovation Project) (Grant No. 2020CXGC010904).

Data Availability Statement: Not applicable.

Acknowledgments: The authors would like to acknowledge thank Zongyao Sun for his comments on this paper and the language revising with Andi Liu.

Conflicts of Interest: The authors declare no conflict of interest.

References

- Oke, T.R. The energetic basis of the urban heat island. *Q. J. R. Meteorol. Soc.* **1982**, *108*, 1–24. [[CrossRef](#)]
- Yao, R.; Wang, L.; Huang, X.; Niu, Z.; Liu, F.; Wang, Q. Temporal trends of surface urban heat islands and associated determinants in major Chinese cities. *Sci. Total Environ.* **2017**, *609*, 742–754. [[CrossRef](#)] [[PubMed](#)]
- Dai, Z.X.; Guldmann, J.M.; Hu, Y.F. Spatial regression models of park and land-use impacts on the urban heat island in central Beijing. *Sci. Total Environ.* **2018**, *626*, 1136–1147. [[CrossRef](#)]
- Yang, J.; Sun, J.; Ge, Q.; Li, X. Assessing the impacts of urbanization-associated green space on urban land surface temperature: A case study of Dalian, China. *Urban For. Urban Green.* **2017**, *22*, 1–10. [[CrossRef](#)]
- Qiao, Z.; Xu, X.; Luo, W.; Wang, F.; Luo, L.; Sun, Z. Urban ventilation network model: A case study of the core zone of capital function in Beijing metropolitan area. *J. Clean. Prod.* **2017**, *168*, 526–535. [[CrossRef](#)]
- Ma, Q.; Wu, J.; He, C. A hierarchical analysis of the relationship between urban impervious surfaces and land surface temperatures: Spatial scale dependence, temporal variations, and bioclimatic modulation. *Landsc. Ecol.* **2016**, *31*, 1139–1153. [[CrossRef](#)]
- Yang, J.; Wang, Y.; Xue, B.; Li, Y.; Xiao, X.; Xia, J.; He, B. Contribution of urban ventilation to the thermal environment and urban energy demand: Different climate background perspectives. *Sci. Total Environ.* **2021**, *795*, 148791. [[CrossRef](#)]
- Veena, K.; Parammasivam, K.M.; Venkatesh, T.N. Urban Heat Island studies: Current status in India and a comparison with the International studies. *J. Earth Syst. Sci.* **2020**, *129*, 85. [[CrossRef](#)]
- Rizwan, A.M.; Dennis, L.Y.C.; Liu, C. A review on the generation, determination and mitigation of Urban Heat Island. *J. Environ. Sci.* **2008**, *20*, 120–128. [[CrossRef](#)]
- Kuang, W.; Yang, T.; Liu, A.; Zhang, C.; Lu, D.; Chi, W. An EcoCity model for regulating urban land cover structure and thermal environment: Taking Beijing as an example. *Sci. China Earth Sci.* **2017**, *60*, 1098–1109. [[CrossRef](#)]
- Wang, Y.; Akbari, H. Analysis of urban heat island phenomenon and mitigation solutions evaluation for Montreal. *Sustain. Cities Soc.* **2016**, *26*, 438–446. [[CrossRef](#)]
- Chakraborty, T.; Hsu, A.; Manya, D.; Sheriff, G. A spatially explicit surface urban heat island database for the United States: Characterization, uncertainties, and possible applications. *ISPRS J. Photogramm. Remote Sens.* **2020**, *168*, 74–88. [[CrossRef](#)]

13. Botje, D.; Dewan, A.; Chakraborty, T.C. Comparing Coarse-Resolution Land Surface Temperature Products over Western Australia. *Remote Sens.* **2022**, *14*, 2296. [[CrossRef](#)]
14. Sobrino, J.A.; Jiménez-Muñoz, J.C.; Paolini, L. Land surface temperature retrieval from LANDSAT TM 5. *Remote Sens. Environ.* **2004**, *90*, 434–440. [[CrossRef](#)]
15. Chang, Y.; Xiao, J.; Li, X.; Middel, A.; Zhang, Y.; Gu, Z.; Wu, Y.; He, S. Exploring diurnal thermal variations in urban local climate zones with ECOSTRESS land surface temperature data. *Remote Sens. Environ.* **2021**, *263*, 112544. [[CrossRef](#)]
16. Yao, L.; Xu, Y.; Zhang, B. Effect of urban function and landscape structure on the urban heat island phenomenon in Beijing, China. *Landsc. Ecol. Eng.* **2019**, *15*, 379–390. [[CrossRef](#)]
17. Meng, Q.; Zhang, L.; Sun, Z.; Meng, F.; Wang, L.; Sun, Y. Characterizing spatial and temporal trends of surface urban heat island effect in an urban main built-up area: A 12-year case study in Beijing, China. *Remote Sens. Environ.* **2018**, *204*, 826–837. [[CrossRef](#)]
18. Zhao, L.; Lee, X.; Smith, R.B.; Oleson, K. Strong contributions of local background climate to urban heat islands. *Nature* **2014**, *511*, 216–219. [[CrossRef](#)]
19. Chakraborty, T.C.; Lee, X.; Ermida, S.; Zhan, W. On the land emissivity assumption and Landsat-derived surface urban heat islands: A global analysis. *Remote Sens. Environ.* **2021**, *265*, 112682. [[CrossRef](#)]
20. Guo, L.; Liu, R.; Men, C.; Wang, Q.; Miao, Y.; Zhang, Y. Quantifying and simulating landscape composition and pattern impacts on land surface temperature: A decadal study of the rapidly urbanizing city of Beijing, China. *Sci. Total Environ.* **2019**, *654*, 430–440. [[CrossRef](#)]
21. Zhou, X.; Chen, H. Impact of urbanization-related land use land cover changes and urban morphology changes on the urban heat island phenomenon. *Sci. Total Environ.* **2018**, *635*, 1467–1476. [[CrossRef](#)] [[PubMed](#)]
22. Qiao, Z.; Tian, G.; Xiao, L. Diurnal and seasonal impacts of urbanization on the urban thermal environment: A case study of Beijing using MODIS data. *ISPRS J. Photogramm. Remote Sens.* **2013**, *85*, 93–101. [[CrossRef](#)]
23. Estoque, R.C.; Murayama, Y.; Myint, S.W. Effects of landscape composition and pattern on land surface temperature: An urban heat island study in the megacities of Southeast Asia. *Sci. Total Environ.* **2017**, *577*, 349–359. [[CrossRef](#)] [[PubMed](#)]
24. Yao, N.; Huang, C.; Yang, J.; Konijnendijk van den Bosch, C.C.; Ma, L.; Jia, Z. Combined Effects of Impervious Surface Change and Large-Scale Afforestation on the Surface Urban Heat Island Intensity of Beijing, China Based on Remote Sensing Analysis. *Remote Sens.* **2020**, *12*, 3906. [[CrossRef](#)]
25. Dai, Z.; Guldmann, J.-M.; Hu, Y. Thermal impacts of greenery, water, and impervious structures in Beijing’s Olympic area: A spatial regression approach. *Ecol. Indic.* **2019**, *97*, 77–88. [[CrossRef](#)]
26. Yang, J.; Zhan, Y.; Xiao, X.; Xia, J.C.; Sun, W.; Li, X. Investigating the diversity of land surface temperature characteristics in different scale cities based on local climate zones. *Urban Clim.* **2020**, *34*, 100700. [[CrossRef](#)]
27. Hu, Y.; Dai, Z.; Guldmann, J.-M. Greenspace configuration impact on the urban heat island in the Olympic Area of Beijing. *Environ. Sci. Pollut. Res.* **2021**, *28*, 33096–33107. [[CrossRef](#)]
28. Norton, B.A.; Coutts, A.M.; Livesley, S.J.; Harris, R.J.; Hunter, A.M.; Williams, N.S.G. Planning for cooler cities: A framework to prioritise green infrastructure to mitigate high temperatures in urban landscapes. *Landsc. Urban Plan.* **2015**, *134*, 127–138. [[CrossRef](#)]
29. Kowe, P.; Mutanga, O.; Odindi, J. Effect of landscape pattern and spatial configuration of vegetation patches on urban warming and cooling in Harare metropolitan city, Zimbabwe. *GIScience Remote Sens.* **2021**, *58*, 261–280. [[CrossRef](#)]
30. Qian, Y.; Zhou, W.; Hu, X.; Fu, F. The Heterogeneity of Air Temperature in Urban Residential Neighborhoods and Its Relationship with the Surrounding Greenspace. *Remote Sens.* **2018**, *10*, 965. [[CrossRef](#)]
31. O’Malley, C.; Piroozfar, P.; Farr, E.R.P.; Pomponi, F. Urban Heat Island (UHI) mitigating strategies: A case-based comparative analysis. *Sustain. Cities Soc.* **2015**, *19*, 222–235. [[CrossRef](#)]
32. Masoudi, M.; Tan, P.Y. Multi-year comparison of the effects of spatial pattern of urban green spaces on urban land surface temperature. *Landsc. Urban Plan.* **2019**, *184*, 44–58. [[CrossRef](#)]
33. Peng, J.; Dan, Y.; Qiao, R.; Liu, Y.; Dong, J.; Wu, J. How to quantify the cooling effect of urban parks? Linking maximum and accumulation perspectives. *Remote Sens. Environ.* **2021**, *252*, 112135. [[CrossRef](#)]
34. Wu, S.; Yang, H.; Luo, P.; Chuan, L.; Li, H.; Liu, M.; Ruan, Y.; Zhang, S.; Xiang, P.; Jia, H.; et al. The effects of the cooling efficiency of urban wetlands in an inland megacity: A case study of Chengdu, Southwest China. *Build. Environ.* **2021**, *204*, 108128. [[CrossRef](#)]
35. Xu, X.L.; Cai, H.Y.; Qiao, Z.; Wang, L.; Jin, C.; Ge, Y.N.; Wang, L.Y.; Xu, F.J. Impacts of park landscape structure on thermal environment using QuickBird and Landsat images. *Chin. Geogr. Sci.* **2017**, *27*, 818–826. [[CrossRef](#)]
36. Feng, X.; Myint, S.W. Exploring the effect of neighboring land cover pattern on land surface temperature of central building objects. *Build. Environ.* **2016**, *95*, 346–354. [[CrossRef](#)]
37. Xiao, X.D.; Dong, L.; Yan, H.N.; Yang, N.; Xiong, Y.M. The influence of the spatial characteristics of urban green space on the urban heat island effect in Suzhou Industrial Park. *Sustain. Cities Soc.* **2018**, *40*, 428–439. [[CrossRef](#)]
38. Boussetta, S.; Balsamo, G.; Dutra, E.; Beljaars, A.; Albergel, C. Assimilation of surface albedo and vegetation states from satellite observations and their impact on numerical weather prediction. *Remote Sens. Environ.* **2015**, *163*, 111–126. [[CrossRef](#)]
39. Weng, Q.; Lu, D.; Schubring, J. Estimation of land surface temperature–vegetation abundance relationship for urban heat island studies. *Remote Sens. Environ.* **2004**, *89*, 467–483. [[CrossRef](#)]
40. Cai, Y.; Chen, Y.; Tong, C. Spatiotemporal evolution of urban green space and its impact on the urban thermal environment based on remote sensing data: A case study of Fuzhou City, China. *Urban For. Urban Green.* **2019**, *41*, 333–343. [[CrossRef](#)]

41. Ke, X.; Men, H.; Zhou, T.; Li, Z.; Zhu, F. Variance of the impact of urban green space on the urban heat island effect among different urban functional zones: A case study in Wuhan. *Urban For. Urban Green.* **2021**, *62*, 127159. [[CrossRef](#)]
42. Zhou, W.; Cao, F. Effects of changing spatial extent on the relationship between urban forest patterns and land surface temperature. *Ecol. Indic.* **2020**, *109*, 105778. [[CrossRef](#)]
43. Li, X.; Zhou, W.; Ouyang, Z. Relationship between land surface temperature and spatial pattern of greenspace: What are the effects of spatial resolution? *Landsc. Urban Plan.* **2013**, *114*, 1–8. [[CrossRef](#)]
44. Zhang, X.; Zhong, T.; Feng, X.; Wang, K.E. Estimation of the relationship between vegetation patches and urban land surface temperature with remote sensing. *Int. J. Remote Sens.* **2009**, *30*, 2105–2118. [[CrossRef](#)]
45. Kong, F.; Yin, H.; James, P.; Hutyrá, L.R.; He, H.S. Effects of spatial pattern of greenspace on urban cooling in a large metropolitan area of eastern China. *Landsc. Urban Plan.* **2014**, *128*, 35–47. [[CrossRef](#)]
46. Asgarian, A.; Amiri, B.J.; Sakieh, Y. Assessing the effect of green cover spatial patterns on urban land surface temperature using landscape metrics approach. *Urban Ecosyst.* **2015**, *18*, 209–222. [[CrossRef](#)]
47. Chen, A.; Yao, L.; Sun, R.; Chen, L. How many metrics are required to identify the effects of the landscape pattern on land surface temperature? *Ecol. Indic.* **2014**, *45*, 424–433. [[CrossRef](#)]
48. Zhou, W.; Huang, G.; Cadenasso, M.L. Does spatial configuration matter? Understanding the effects of land cover pattern on land surface temperature in urban landscapes. *Landsc. Urban Plan.* **2011**, *102*, 54–63. [[CrossRef](#)]
49. Xu, C.; Chen, G.D.; Huang, Q.Y.; Su, M.R.; Rong, Q.Q.; Yue, W.C.; Haase, D. Can improving the spatial equity of urban green space mitigate the effect of urban heat islands? An empirical study. *Sci. Total Environ.* **2022**, *841*, 156687. [[CrossRef](#)]
50. Rahaman, Z.A.; Kafy, A.A.; Saha, M.; Rahim, A.A.; Almulhim, A.I.; Rahaman, S.N.; Fattah, M.A.; Rahman, M.T.; Kalaivani, S.; Faisal, A.-A.; et al. Assessing the impacts of vegetation cover loss on surface temperature, urban heat island and carbon emission in Penang city, Malaysia. *Build. Environ.* **2022**, *222*, 109335. [[CrossRef](#)]
51. Yao, L.; Li, T.; Xu, M.; Xu, Y. How the landscape features of urban green space impact seasonal land surface temperatures at a city-block-scale: An urban heat island study in Beijing, China. *Urban For. Urban Green.* **2020**, *52*, 126704. [[CrossRef](#)]
52. Maimaitiyiming, M.; Ghulam, A.; Tiyyip, T.; Pla, F.; Latorre-Carmona, P.; Halik, Ü.; Sawut, M.; Caetano, M. Effects of green space spatial pattern on land surface temperature: Implications for sustainable urban planning and climate change adaptation. *ISPRS J. Photogramm. Remote Sens.* **2014**, *89*, 59–66. [[CrossRef](#)]
53. Han, D.; Yang, X.; Cai, H.; Xu, X. Impacts of Neighboring Buildings on the Cold Island Effect of Central Parks: A Case Study of Beijing, China. *Sustainability* **2020**, *12*, 9499.
54. Yang, J.; Wang, Y.; Xiao, X.; Jin, C.; Xia, J.; Li, X. Spatial differentiation of urban wind and thermal environment in different grid sizes. *Urban Clim.* **2019**, *28*, 100458. [[CrossRef](#)]
55. Yang, J.; Yang, Y.; Sun, D.; Jin, C.; Xiao, X. Influence of urban morphological characteristics on thermal environment. *Sustain. Cities Soc.* **2021**, *72*, 103045. [[CrossRef](#)]
56. Qiao, Z.; Wu, C.; Zhao, D.; Xu, X.; Yang, J.; Feng, L.; Sun, Z.; Liu, L. Determining the Boundary and Probability of Surface Urban Heat Island Footprint Based on a Logistic Model. *Remote Sens.* **2019**, *11*, 1368. [[CrossRef](#)]
57. Di, S.; Li, Z.L.; Tang, R.; Pan, X.; Liu, H.; Niu, Y. Urban green space classification and water consumption analysis with remote-sensing technology: A case study in Beijing, China. *Int. J. Remote Sens.* **2019**, *40*, 1909–1929. [[CrossRef](#)]
58. Hirata, Y.; Takahashi, T. Image segmentation and classification of Landsat Thematic Mapper data using a sampling approach for forest cover assessment. *Can. J. For. Res.* **2011**, *41*, 35–43. [[CrossRef](#)]
59. Qin, Z.; Li, W.; Xu, B.; Chen, Z.; Liu, J. The Estimation of Land Surface Emissivity for Landsat TM6. *Remote Sens. Land Resour.* **2004**, *16*, 28–32. [[CrossRef](#)]
60. Park, C.Y.; Park, Y.; Kim, H.; Yun, S.; Kim, C.-K. Quantifying and Mapping Cooling Services of Multiple Ecosystems. *Sustain. Cities Soc.* **2021**, *73*, 103123. [[CrossRef](#)]
61. Park, J.; Kim, J.-H.; Lee, D.K.; Park, C.Y.; Jeong, S. The influence of small green space type and structure at the street level on urban heat island mitigation. *Urban For. Urban Green.* **2017**, *21*, 203–212. [[CrossRef](#)]
62. Chen, X.-L.; Zhao, H.-M.; Li, P.-X.; Yin, Z.-Y. Remote sensing image-based analysis of the relationship between urban heat island and land use/cover changes. *Remote Sens. Environ.* **2006**, *104*, 133–146. [[CrossRef](#)]
63. Zhao, M.Y.; Cai, H.Y.; Qiao, Z.; Xu, X.L. Influence of urban expansion on the urban heat island effect in Shanghai. *Int. J. Geogr. Inf. Sci.* **2016**, *30*, 2421–2441. [[CrossRef](#)]
64. Jamei, Y.; Rajagopalan, P.; Sun, Q. Spatial structure of surface urban heat island and its relationship with vegetation and built-up areas in Melbourne, Australia. *Sci. Total Environ.* **2019**, *659*, 1335–1351. [[CrossRef](#)] [[PubMed](#)]
65. Chapman, S.; Thatcher, M.; Salazar, A.; Watson, J.E.M.; McAlpine, C.A. The Effect of Urban Density and Vegetation Cover on the Heat Island of a Subtropical City. *J. Appl. Meteorol. Climatol.* **2018**, *57*, 2531–2550. [[CrossRef](#)]
66. Li, X.; Zhou, W. Optimizing urban greenspace spatial pattern to mitigate urban heat island effects: Extending understanding from local to the city scale. *Urban For. Urban Green.* **2019**, *41*, 255–263. [[CrossRef](#)]
67. Takayama, N.; Yamamoto, H.; Iwaya, K.; Fei, W.; Harada, Y.; Higashiyama, M.; Tsuchiya, Y.; Kaneishi, A.; Shirozu, T. Quantitative Evaluation of Urban Heat Island Mitigation Effect and Reduction Human Heat Stress by Large Greening of Roof. *J. Agric. Meteorol.* **2008**, *64*, 257–270. [[CrossRef](#)]
68. Rupasinghe, H.T.; Halwatura, R.U. Benefits of implementing vertical greening in tropical climates. *Urban For. Urban Green.* **2020**, *53*, 126708. [[CrossRef](#)]

69. Peng, L.; Jim, C. Green-Roof Effects on Neighborhood Microclimate and Human Thermal Sensation. *Energies* **2013**, *6*, 598–618.
70. Maheng, D.; Ducton, I.; Lauwaet, D.; Zevenbergen, C.; Pathirana, A. The Sensitivity of Urban Heat Island to Urban Green Space—A Model-Based Study of City of Colombo, Sri Lanka. *Atmosphere* **2019**, *10*, 151. [[CrossRef](#)]
71. Song, J.; Du, S.; Feng, X.; Guo, L. The relationships between landscape compositions and land surface temperature: Quantifying their resolution sensitivity with spatial regression models. *Landsc. Urban Plan.* **2014**, *123*, 145–157. [[CrossRef](#)]
72. He, B.-J.; Ding, L.; Prasad, D. Wind-sensitive urban planning and design: Precinct ventilation performance and its potential for local warming mitigation in an open midrise gridiron precinct. *J. Build. Eng.* **2019**, *29*, 101145. [[CrossRef](#)]
73. He, B.-J.; Ding, L.; Prasad, D. Enhancing urban ventilation performance through the development of precinct ventilation zones: A case study based on the Greater Sydney, Australia. *Sustain. Cities Soc.* **2019**, *47*, 101472. [[CrossRef](#)]
74. Yang, J.; Wang, Y.; Xiu, C.; Xiao, X.; Xia, J.; Jin, C. Optimizing local climate zones to mitigate urban heat island effect in human settlements. *J. Clean. Prod.* **2020**, *275*, 123767. [[CrossRef](#)]
75. Yang, P.; Ren, G.; Yan, P. Evidence for a Strong Association of Short-Duration Intense Rainfall with Urbanization in the Beijing Urban Area. *J. Clim.* **2017**, *30*, 5851–5870. [[CrossRef](#)]
76. Kedia, S.; Bhakare, S.P.; Dwivedi, A.K.; Islam, S.; Kagainalkar, A. Estimates of change in surface meteorology and urban heat island over northwest India: Impact of urbanization. *Urban Clim.* **2021**, *36*, 100782. [[CrossRef](#)]